ChemComm

COMMUNICATION

View Article Online
View Journal | View Issue

Cite this: *Chem. Commun.*, 2021, 57, 879

Received 5th November 2020,
Accepted 9th December 2020

DOI: 10.1039/d0cc07303b

rsc.li/chemcomm

A nickel oxide-decorated *in situ* grown 3-D graphitic forest engrained carbon foam electrode for microbial fuel cells†

Shiv Singh, ‡*[a] Amol Pophali,‡[b] Rishabh Anand Omar,[b] Rajeev Kumar,[a] Pradip Kumar,[c] Dehi Pada Mondal,[a] Deepak Pant *[d] and Nishith Verma *[b]

A facile and single-step nickel oxide-dispersed *in situ* grown 3-D graphitic forest engrained carbon foam (NiO-CNF-CF)-based electrode was fabricated for high-performance microbial fuel cells (MFCs). The metal oxide, graphitic contents, biocompatibility, stability and large surface area available in the material for biofilm formation rendered the prepared electrode competent for wastewater treatment and bioenergy (0.79 V and 1.955 W m^{-2}) generation with a coulombic efficiency of 85.66%.

Microbial fuel cells (MFCs) exploit exoelectrogenic bacteria to utilize the chemical energy of biodegradable organic compounds, transforming it to electrical energy. The exoelectrogens recover the energy from complex organic matter present more efficiently in MFCs than in the other chemical fuel cells. Apart from energy generation, the MFCs also treat wastewater *via* COD reduction.[1–3] Thousands of research articles are published each year for optimizing the various operating parameters of an MFC for scale-up, including configuration, compositions of electrolyte, types of ion exchange membrane, biocatalyst (exoelectrogens), and electrode materials.[1,4,5] Notwithstanding such attempts, low energy output and expensive electrodes continue to be the main hurdles in commercialization of MFCs.[6]

Studies reveal that the types of electrodes and their spatial orientations directly affect the efficacy of MFCs. Graphitic carbon-based porous or non-porous electrodes such as carbon nanotubes (CNTs), carbon nanofibers (CNFs), reduced graphene oxides (rGO), graphene, graphitic carbon brush, and graphitic felt, disks, or rods are considered to be more competent anodes among all types of currently available electrode materials.[7,8] These anode materials possess a high surface area for biofilm formation, and are biocompatible, chemically/mechanically stable, conductive for electron transport from exoelectrogen bacteria, and comparatively economical. A few studies have revealed that the electricity generation in MFCs is directly proportional to the concentration and development rate of exoelectrogen.[9] An extensive research study has also been performed on the fabrication of cathodes for efficient oxygen reduction reaction (ORR) and lowering the overpotential of oxygen.[10,11] In this context, graphitic carbon doped with noble/transition metal or metal oxide nanoparticles (Pt, Mn, Sn, W, Au, Ru, Ni, Ti, *etc.*) has been commonly used.[8,12,13]

In the recent past, electrodes with a 3-D open-porous structure have been fabricated to enhance MFC performance. However, despite their promising results, many 3-D materials (graphene foam, CNT-coated sponges, *etc.*) have some drawbacks such as biocompatibility and high cost.[14] Thus, high-quality electrodes with good electrical conductivity, biocompatibility, large surface area, and low fabrication cost are in high demand. With a view to meeting such attributes of a high-quality electrode, the present study focuses on the development of nickel oxide (NiO)-dispersed *in situ* grown 3-D CNFs engrained carbon foam (CF) and its application as an electrode in a double-chambered MFC. The NiO nanoparticles dispersed in NiO-CNF-CF play multiple roles, *viz.*, a catalyst for the ORR at the cathode, a facilitator of electron transfer within the electrode surface, and a catalyst for the growth of the CNFs during fabrication. The graphitic CNFs enhance the electroconductivity, and also provide biocompatibility, and active sites for the efficient growth of a biofilm. Moreover, the high electrical and thermal conductivity of CF render it a suitable candidate for the substrate material. The CF substrate was prepared as per the

[a] *Lightweight metallic materials, Council of Scientific and Industrial Research-Advanced Materials and Processes Research Institute, Bhopal-462026, India. E-mail: sshiv.singh@ampri,res.in, sshiviitk@gmail.com*
[b] *Department of Chemical Engineering, Indian Institute of Technology Kanpur, Kanpur-208016, India. E-mail: nishith@iitk.ac.in*
[c] *Integrated Approach for Design and Product Development Division, CSIR-Advanced Materials and Processes Research Institute, Habibganj Naka, Hoshangabad Road, Bhopal, Madhya Pradesh, 462026, India*
[d] *Separation & Conversion Technology, Flemish Institute for Technological Research (VITO), Boeretang 200, Mol 2400, Belgium. E-mail: deepak.pant@vito.be*

† Electronic supplementary information (ESI) available: Additional information on fabrication, characterization of the 3-D graphitic forest engrained carbon foam and MFC set-up and operation. See DOI: 10.1039/d0cc07303b

‡ These authors contributed equally to this work.

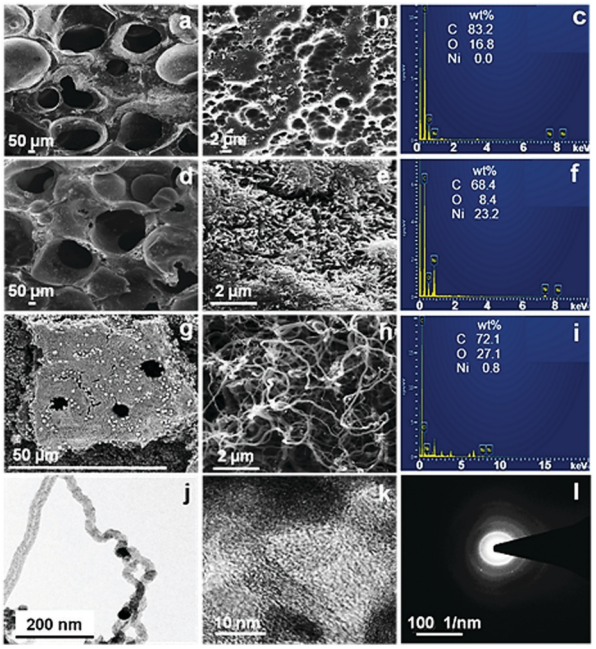

Fig. 1 SEM and EDX micrographs of (a–c) CF, (d–f) NiO-CF, and (g–i) NiO-CNF-CF. TEM images of NiO-CNF-CF at (j) low and (k) high resolutions, and (l) the corresponding SAED pattern.

previously described protocol [ESI†].[15] The prepared CF samples were impregnated with 0.4 M nickel nitrate hexahydrate salt solution. The solution contained 0.3% (w/w) sodium dodecyl sulfate as the anionic surfactant to prevent agglomeration of the Ni-salt, and enhance the metal loading in CF. The salt-impregnated samples are dried at room temperature (30 ± 5 °C) for 10 h and calcined at 400 °C for 4 h under N_2 flow (200 sccm) to synthesize NiO-CF. Finally, the CNFs were grown over NiO-CF by subjecting it to chemical vapor deposition (CVD) at 650 °C for 2 h, and the NiO-CNF-CF electrode was fabricated.

The morphology of the prepared electrode samples was observed using scanning electron microscopy (SEM) (MIRA-3, TESCAN, Brno, Czech Republic). Fig. 1a and b show a SEM image of the CF sample, which confirms the existence of a distinct meso–macroporous structure in the material. Such bimodal pore structure would ease the diffusion of ions from the electrolyte to the material pores. The SEM image (Fig. 1d) of NiO-CF shows a large number of quasi-uniform flaked spike-like structures over the CF. The high magnification-SEM images (Fig. 1e) reveal that the spikes are formed from many flexible and densely interlaced nanoparticles. Since these structures are self-built from the NiO nanoparticles, formation of the spongy assembly (addressed further) could be facilitated by the inter-aggregation of the building blocks.[16,17] Furthermore, the SEM image of NiO-CNF-CF (Fig. 1g) shows the coverage of the electrode surface by CNFs.

The high magnification image (Fig. 1h) confirms dense CNF-forest growth *via* the tip-growth mechanism.[18] Fig. 1b, e and h also show a clear transition in the porosity from CF to NiO-CNF-CF, discussed later. The energy-dispersive X-ray (EDX) spectra (JSM-7100 F, JEOL, USA) of CF confirmed the presence of C and O in the material (Fig. 1c). Also, the EDX spectra of NiO-CF (Fig. 1f) and NiO-CNF-CF (Fig. 1i) confirmed the presence of Ni in the respective materials. The elemental mapping (Fig. S1, ESI†) of the electrodes showed uniform distribution of the elements at the surface and the data are in agreement with the EDX spectra. The microstructure of NiO-CNF-CF was visually observed using transmission electron microscopy (TEM) (FEI-Tecnai G2 12 Twin TEM 120 kV). In Fig. 1j, the dark spots represent the NiO nanoparticles on the tips of the CNFs. The high-resolution TEM (HR-TEM) image showed the polycrystalline NiO lattices and graphitic carbon fringes (Fig. 1k). The fringe width of the phases in the HR-TEM image is described in Fig. S2 (ESI†). The selected area diffraction (SAED) pattern also showed the co-existence of NiO and CNFs (Fig. 1l). The dotted diffraction rings confirmed the polycrystalline characteristics of NiO, whereas the hazy rings represented the characteristics of amorphous carbon in the CNFs. The prepared samples (CF, NiO-CF, NiO-CNF-CF) were further characterized using X-ray diffraction (XRD) (PANalytical, X'Pert-Pro) to determine the different phases in the materials. The XRD spectra (Fig. 2a) exhibit the common characteristic peaks at $2\theta \sim 26^\circ$ for the amorphous and crystalline phases, and at 44.1° for the crystallographic planes of the hexagonal structure, corresponding to the (0 0 2) and (1 0 1) indices, respectively, in the materials (JCPDS No. 00-041-1487). The peak intensity was relatively higher in NiO-CNF-CF, as the inclusion of the CNFs increased the total graphitic carbon content, confirmed later using Raman spectroscopy. The presence of Ni (in any chemical state) was confirmed in NiO-CF and NiO-CNF-CF, whereas it was absent in CF. The peak characteristics of NiO at $2\theta \sim 37.2$, 43.3, and 75.4° corresponding to the (1 1 1), (2 0 0) and (3 1 1) crystallographic planes, respectively (JCPDS No. 00-047-1049) with a cubic structure, while those of Ni at $2\theta \sim 44.5$, 53.3, and 76.3° corresponding to the (1 1 1), (2 0 0) and (2 2 0) crystallographic planes,

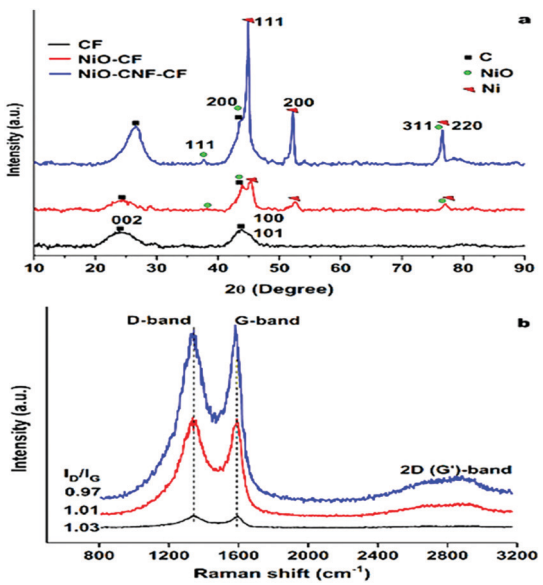

Fig. 2 (a) XRD and (b) Raman spectra of CF, NiO-CF and NiO-CNF-CF electrodes.

respectively (JCPDS No. 04-0850) in an FCC phase were confirmed from Fig. 2a. The crystallite size of the NiO and Ni nanoparticles, calculated using the Scherrer formula, was found to be in the range 20.5–56.1 nm and 37.3–56.4 nm, respectively. The peak-intensity of zero-valent Ni increased post CVD process, *i.e.*, in NiO-CNF-CF. No foreign peaks, *viz.* other than those for Ni/NiO and carbon, were detected in the XRD spectra, indicating complete transformation of Ni salt to NiO, post calcination step. The XRD data were also verified using the high resolution TEM image (Fig. S2, ESI†).

Raman spectroscopy (Model: Alpha, Make: Witec, Germany) analysis was performed to determine the molecular structure and bonding vibration in the prepared materials. Two vibrational peaks were observed: (1) at $\sim$ 1342 cm^{-1} corresponding to the disordered sp^2 carbon networks or defects in the graphitic structure (D-band), (2) at $\sim$1590 cm^{-1} corresponding to the ordered sp^2 structure or graphitic phase (G-band) (Fig. 2b). The I_D/I_G ratio represents the relative amounts of disorderedness and graphitic content in the sample. The I_D/I_G ratios are in the following order: 0.97 (NiO-CNF-CF) $<$ 1.01 (NiO-CF) $<$ 1.03 (CF). Therefore, NiO-CNF-CF may be considered to be containing the greatest graphitic phase concentration amongst the prepared three electrode materials (consistent with XRD data), which is likely to enhance the conductivity of the material and electrochemical performance, addressed later. Thermogravimetric analysis (TGA) (Toledo-Mettler, USA) of the electrodes was performed to check their thermal stability in the synthesis process (Fig. S3a, ESI†). The compressive strength of the electrodes was also tested, and NiO-CNF-CF carried 40% more load compared to that on CF (Fig. S3b, ESI†). Thus, NiO-CNF-CF was found to be thermally and physically stable. The associated porosity in the materials was studied using BET analysis (Autosorb-1C Quantachrome instrument, USA), and the data are presented in Table S1 (ESI†). As shown, NiO-CNF-CF was mostly microporous.

The electrochemical response of the prepared electrodes was determined in a three-electrode cell assembly contained with a 10 mM-phosphate buffer solution (PBS), and connected to the potentiostat (AUTOLAB-PGSTAT302N). Cyclic voltammograms (CV) for NiO-CNF-CF were recorded at different scan rates over the voltage range -1.0 to 1.0 V (Fig. S4a, ESI†), and the optimized value of 50 mV s^{-1} was used for further analysis. Fig. 3a shows CV plots of the electrode materials. The CV curve for CF displays a characteristic electrochemical double-layer capacitance (EDLC) type behaviour with low current values and area between the cycles.[19] The CV plot for NiO-CF showed the same characteristics with increased currents and areas between the curves, attributed to the material porosity. However, the visible redox peaks in the CV plot of NiO-CNF-CF indicate the pseudocapacitive contribution in addition to the EDLC mechanism.[19] The electrocatalytic properties of CNFs and NiO nanoparticles contributed to the faradaic current, while the porosity was responsible for the capacitive current. Moreover, the current values and areas between the cathodic and anodic sweep significantly increased, indicating a superior electrochemical activity of the electrode. A CV analysis of NiO-CNF (without CF) was performed to check its catalytic activity.

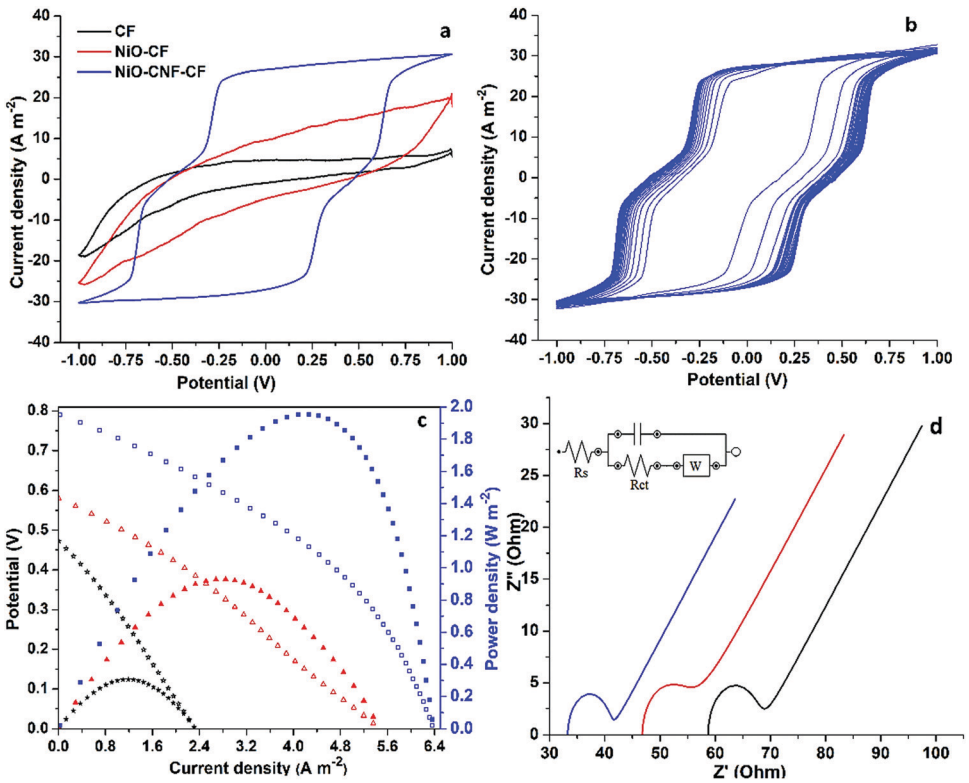

Fig. 3 Electrochemical analysis including (a) CV, (b) multi-cycle CV, (c) polarization data, and (d) EIS analysis of the prepared electrodes.

For this, NiO-CNF was coated over the glassy carbon electrode, and a clear reduction peak was observed (Fig. S4b, ESI†). Thus, the EDLC behaviour in the electrodes was confirmed *via* the material porosity. A 50 cycle CV (Fig. 3b) was performed to demonstrate the electrochemical stability of NiO-CNF-CF, and the electrode exhibited an approximately similar response throughout all cycles. Therefore, NiO-CNF-CF is electrochemically stable and could be used for a long duration. A double-chambered MFC was used to carry out the MFC operations. Fabrication of MFC is described in one of our previous studies.[4] The replacement of the wastewater sample (COD: 11 200 mg L^{-1}), collected from the Panki Thermal Power Plant, Kanpur (U.P.), India, as the anolyte, and the arrangement of electrodes directly connected to a Teflon-coated copper wire assembly were slight modifications to mention. Fig. 3c shows the polarization and power density plots based on the MFC test data. The tests were performed in three batches: (1) CF, (2) NiO-CF and (3) NiO-CNF-CF as the MFC electrodes. In batch 1 and 2, the open circuit potential (OCP), maximum current density and maximum power density were measured to be ~0.472 V, 2.32 A m^{-2} and 0.306 W m^{-2}, and ~0.58 V, 5.455 A m^{-2} and 0.928 W m^{-2}, respectively. On the other hand, batch 3 using NiO-CNF-CF as the electrodes recorded the OCP, maximum current density and maximum power density of ~0.79 V, 6.381 A m^{-2} and 1.955 W m^{-2}, respectively. Clearly, the presence of NiO and CNF in NiO-CNF-CF contributed to its superior electrocatalytic activity than CF. Electrochemical impedance spectroscopy (EIS) analysis was also performed to determine the voltage losses in the MFC. Fig. 3d shows the Nyquist plots for the batch studies. The EIS plots are represented by a semi-circle and a straight line. The semicircle is formed because of the charge transfer (R_{ct}) and capacitive resistances (C is the height of the semicircle towards Y axis), whereas the straight line thus formed is because of the diffusion resistance characterized by the Warburg mass transfer resistance (W). The double layer capacitance is in parallel with R_{ct} and W, which together are in series with R_s. Thus, the performance of MFC depends on both the charge transfer and mass transfer resistance. In addition to these, the solution resistance (R_s) depends on the conductivities of the electrodes and electrolytes, PEM, and various electrical connections. The calculated values of R_s, R_{ct} and W for the MFC batch based on the CF and NiO-CF electrodes were 58.7, 9.03 and 10.54 Ω, and 46.8, 8.12 and 10.2 Ω, respectively, while those based on the NiO-CNF-CF electrodes were 33.3, 7.62, and 8.06 Ω, respectively. NiO nanoparticles and graphitic CNFs contributed less internal resistance in NiO-CNF-CF than the other two electrodes, and showed more favorable conditions for the formation of a biofilm (Fig. S5, ESI†) and efficient ORR. Notably, the MFC test runs also resulted in the COD reduction of the wastewater in the anode chamber. The MFC set-up based on the CF and NiO-CF electrodes achieved 28.57 and 43.86% COD-reduction, respectively whereas that based on the NiO-CNF-CF electrodes achieved 71.42% reduction. The coulombic efficiency achieved in these batches was 62.63, 71.45 and 85.66%, respectively. The stability and durability of the NiO-CNF-CF electrode were also examined in a three-cycle MFC operation (Fig. S6, ESI†) for ~18 days. A similar trend of cycles and constant voltage output confirmed the electrode to be stable.

In summary, a facile and single-step approach for the synthesis of a novel NiO-CNF-CF electrode was successfully used. The material was confirmed to be porous, electroconductive, and highly graphitic with stable electrocatalytic behaviour. The MFC tests recorded high OCP (~0.79 V), current density (~6.381 A m^{-2}) and power density (~1.955 W m^{-2}) with low internal resistances: R_s (33.3 Ω), R_{ct} (7.62 Ω) and W (8.06 Ω). Also, the MFC operation could reduce 71.42% COD and achieved 85.66% coulombic efficiency. The electrode also proved to be stable for multiple-cycle MFC operation. The combined effects of NiO nanoparticles, graphitic CNFs, the porous structure of the material, and the electrical properties of carbon foam added up to a significantly superior MFC performance. The novel NiO-CNF-CF is a low-cost biocompatible electrocatalyst that can serve as a potential alternative to the existing complex electrodes.

Conflicts of interest

There are no conflicts to declare.

References

1 X. Xie, G. Yu, N. Liu, Z. Bao, C. S. Criddle and Y. Cui, *Energy Environ. Sci.*, 2012, **5**, 6862–6866.
2 H. Wang, G. Wang, Y. Ling, F. Qian, Y. Song, X. Lu, S. Chen, Y. Tong and Y. Li, *Nanoscale*, 2013, **5**, 10283–10290.
3 S. Singh, P. K. Bairagi and N. Verma, *Electrochim. Acta*, 2018, **264**, 119–127.
4 S. Singh and N. Verma, *Int. J. Hydrogen Energy*, 2015, **40**, 5928–5938.
5 A. Modi, S. Singh and N. Verma, *Electrochim. Acta*, 2016, **190**, 620–627.
6 H. Jiang, L. Yang, W. Deng, Y. Tan and Q. Xie, *J. Power Sources*, 2017, **363**, 27–33.
7 X. Xie, M. Ye, L. Hu, N. Liu, J. R. McDonough, W. Chen, H. N. Alshareef, C. S. Criddle and Y. Cui, *Energy Environ. Sci.*, 2012, **5**, 5265–5270.
8 R. Kaur, A. Marwaha, V. A. Chhabra, K.-H. Kim and S. K. Tripathi, *Renewable Sustainable Energy Rev.*, 2020, **119**, 109551.
9 S. Chen, Q. Liu, G. He, Y. Zhou, M. Hanif, X. Peng, S. Wang and H. Hou, *J. Mater. Chem.*, 2012, **22**, 18609–18613.
10 A. J. Slate, K. A. Whitehead, D. A. C. Brownson and C. E. Banks, *Renewable Sustainable Energy Rev.*, 2019, **101**, 60–81.
11 S. Singh, A. Modi and N. Verma, *Int. J. Hydrogen Energy*, 2016, **41**, 1237–1247.
12 S. G. Peera, T. Maiyalagan, C. Liu, S. Ashmath, T. G. Lee, Z. Jiang and S. Mao, *Int. J. Hydrogen Energy*, 2020, DOI: 10.1016/j.ijhydene.2020.07.252.
13 Y. Wu, L. Wang, M. Jin, F. Kong, H. Qi and J. Nan, *Bioresour. Technol.*, 2019, **283**, 129–137.
14 T. H. Han, S. Y. Sawant, S.-J. Hwang and M. H. Cho, *RSC Adv.*, 2016, **6**, 25799–25807.
15 R. Kumar, D. P. Mondal, A. Chaudhary, M. Shafeeq and S. Kumari, *Composites, Part A*, 2018, **112**, 475–484.
16 K. Y. Kumar, H. B. Muralidhara, Y. A. Nayaka, H. Hanumanthappa, M. S. Veena and S. R. K. Kumar, *Bull. Mater. Sci.*, 2015, **38**, 271–282.
17 Q. Luo, M. Peng, X. Sun and A. M. Asiri, *Catal. Sci. Technol.*, 2016, **6**, 1157–1161.
18 R. M. Singhal, A. Sharma and N. Verma, *Ind. Eng. Chem. Res.*, 2008, **47**, 3700–3707.
19 Q. Bai, Y. Shen, T.-A. Asoh, C. Li, Y. Dan and H. Uyama, *Nanoscale*, 2020, **12**, 15261–15274.

